April, 2005

Unsteady Effects on Trailing Edge Cooling

G. Medic, *Stanford University*
Paul A. Durbin, *Stanford University*

G. Medic
P. A. Durbin

Mechanical Engineering Department,
Stanford University,
Stanford, CA 94305-3030

Unsteady Effects on Trailing Edge Cooling

It is shown how natural and forced unsteadiness play a major role in turbine blade trailing edge cooling flows. Reynolds averaged simulations are presented for a surface jet in coflow, resembling the geometry of the pressure side breakout on a turbine blade. Steady computations show very effective cooling; however, when natural—or even moreso, forced—unsteadiness is allowed, the adiabatic effectiveness decreases substantially. Streamwise vortices in the mean flow are found to be the cause of the increased heat transfer. [DOI: 10.1115/1.1860565]

1 Introduction

The trailing edges of high pressure turbine blades are subjected to substantial heat loads. For this reason cooling air is blown from breakouts on the pressure side, jetting toward the trailing edge. A computational analysis has tended to significantly overestimate the cooling effectiveness of these jets. Indeed, adiabatic effectiveness, η, is found to be nearly 1 to the trailing edge; at least, that is so when the predictions in question are steady, Reynolds-averaged (RANS) computations. Unfortunately, lab tests show that the effectiveness starts to drop after about four jet nozzle diameters, and might fall to about 0.5 near the trailing edge, at typical blowing ratios. It has been suggested that the discrepancy between prediction and observation might be due to coherent unsteadiness [1].

In the present paper, we describe unsteady RANS computations of a flow that is representative of the pressure-side, trailing edge. Some interesting phenomenology is observed. It is this, not applied prediction methods, that is the subject of this article. We find that natural unsteadiness does arise, due to three-dimensional vortex shedding from the upper lip of the breakout (Fig. 2, later). This mean flow unsteadiness causes some extra mixing, and causes the time-averaged η to decrease noticeably below 1; however, it does not seem to drop as much as lab tests lead one to expect. Pulsations added to the upstream plenum cause a more substantial drop in η. Adiabatic effectiveness then mimics that observed experimentally. It is unclear whether the pulsations have any analogy to conditions that occur in lab tests; so they are presented here simply as a study in the effect of forcing. A fascinating change in the mean vortical structure is seen under the imposition of periodic forcing. The shed vortices become more three-dimensional, forming into loops, which are the cause of greatly enhanced mixing.

The rationale for unsteady RANS is sometimes a cause of confusion. There is no inconsistency between representing turbulent mixing by a statistical closure, while computing an unsteady mean flow [2]. In the presence of coherent, periodic unsteadiness, the energy spectrum will look like Fig. 1. Mixing due to the broadband portion of the spectrum is represented by the closure model. The spike is due to mean flow unsteadiness. This *must be computed* by an unsteady simulation. It is a source of additional mixing—mixing that is not due to turbulence, but rather, to vortices in the mean flow.

Holloway et al. [3] have previously suggested a role of unsteadiness in the pressure-side bleed problem. Indeed, the present is a follow-on to their study, and is motivated by the same experiments. Those experiments are described in Holloway et al. [1]. The papers by Holloway et al. appear be the only previous computational studies of coherent unsteadiness in external trailing edge film cooling. Computations addressing the passages internal to the trailing edge are discussed in Rigby and Bunker [4]. A recent article by Martini and Shultz [5] describes experiments and computations of a trailing edge geometry, cooled by a row of jets, without lands. They found unsteadiness due to random coalescence between the jets. However, unsteadiness was not important in their CFD analysis. Their geometry differs substantially from the present, because of the lands.

Manuscript received January 21, 2003; revision received November 8, 2004. Review conducted by: S. Acharya.

2 Computations

The commercial code, CFX, was used for the present simulations. Second-order time stepping must be used for this code to capture the coherent unsteadiness. With that switched on, we conducted a number of grid- and time-step refinements to be convinced that the observed unsteadiness is not a numerical artifact. In fact, we ran a few simulations with a different code, Star-CD, with similar results. Hence, the numerical accuracy appears to be sufficient for the task at hand.

The present computations invoke the SST model, as implemented in CFX. The broad features of these simulations are insensitive to the particulars of the turbulence closure; similar results were seen with the two-layer RNG and Chen $k-\epsilon$ models.

Figure 2 shows the computational domain. It consists of an upstream plenum, a land that channels the flow into jets, and an external region of coflowing fluid. At the breakout the internal flow exits through a rectangular nozzle. The thickness of the upper lip of the nozzle is equal to the height of the jet. The land protrudes downstream from the nozzle, in a wedge shape, to the trailing edge. The lower part of Fig. 2 shows a geometry constructed from four images of the domain.

The flow is from left to right, in two streams: the wall jet exits from the plenum and is channeled by the land; the external flow enters in the upper portion. Generally, the two streams have different bulk velocities; their ratio, $U_{\text{jet}}/U_{\text{free-stream}}$ is the blowing ratio, since we consider constant density, incompressible flow. A few compressible simulations showed the same vortical flow components and heat transfer that are described herein.

The geometry is subject to a symmetry condition on the left and the right lateral sides of the domain. This emulates a series of jets, blowing toward the trailing edge. The computational domain contains only one-half of the jet exit; hence the second symmetry condition is at the center of the jet. Computations with a full jet cross section produced very similar results to those shown herein. In the presence of forcing, the flow becomes quite complex. That was the primary motive for testing the validity of the symmetry assumption. The present forcing was plane wave; hence, it is consistent with the symmetry, but it was uncertain whether the flow respects that symmetry—it appears that it does. Therefore, we present results only for the geometry of Fig. 2. The Reynolds number based on free-stream velocity and nozzle lip thickness is 5×10^4.

The final grid consisted of 0.75 million cells, in a block structured form. The solver treats it as fully unstructured, but block

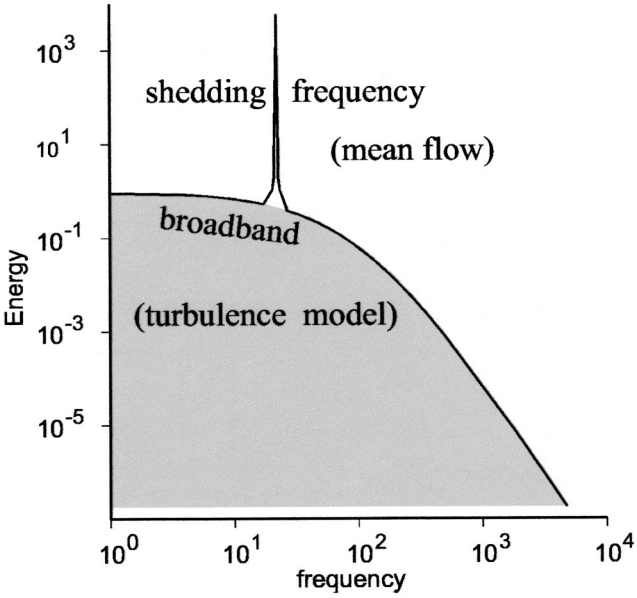

Fig. 1 The form of an energy spectrum with broadband and coherent frequencies. Units are arbitrary.

structured gridding produced a smooth grid, with good resolution near surfaces and in the wake of the upper nozzle lip. A grid refinement study was conducted, with a special focus on the grid blocks in the shedding region. The resolution in those blocks was successively doubled in the streamwise and spanwise direction. The finest grid had 1.25 million cells. Coarsening the grid in the same manner led to a loss of accuracy for grids with approximately 0.25 million cells. The 0.75 million cell mesh was designed from these studies, to provide grid insensitivity.

For the time-accurate computations, the time step was adjusted to provide about $50\Delta t$ per period. In the natural case, no forcing was applied. The flow was allowed to develop a self-sustained unsteadiness. A large number of simulations, not reported herein, were conducted at various blowing ratios. It was found that coherent unsteadiness developed spontaneously for all simulations with a blowing ratio larger than 0.35 (simulations for very low blowing ratios were not performed). For blowing ratios larger than 1.5, the unsteadiness was damped down and the flow became steady. To confirm the computational results, lab tests were conducted on the rig described in Holloway et al. [1] solely to determine whether or not coherent unsteadiness occurred. The results were positive: a frequency was seen corresponding to a Strouhal number of about 0.2.

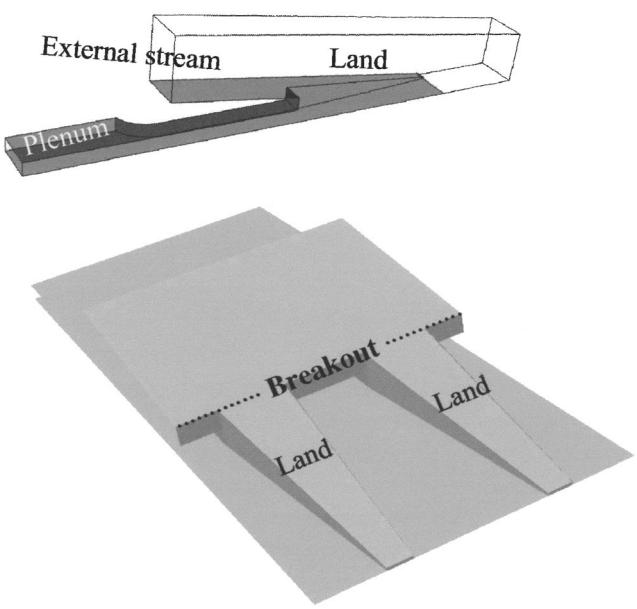

Fig. 2 The computational geometry

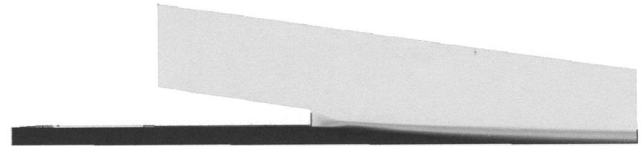

Fig. 3 Temperature contours in steady flow

3 Results

Observations will be summarized for steady, unsteady, and forced simulations. To an extent, we are using a RANS simulation to understand the averaged mixing processes of the pressure-side cooling jets.

Temperature contours in a vertical section through the mid plane of the nozzle shows how a layer of cool fluid lies next to the wall in the steady flow calculation: see Fig. 3. The same midplane section through an unsteady computation shows vortex shedding from the upper nozzle lip: see Fig. 4.

Comparing the temperature contours from the steady (Fig. 3) and unsteady solutions (Fig. 4) shows that the mean flow vortices cause substantial additional mixing. However, a layer of cool air persists next to the wall for a distance of about eight jet heights. The cooling effectiveness,

$$\eta \equiv (T_{\text{hot}} - T_{\text{wall}})/(T_{\text{hot}} - T_{\text{cool}}), \tag{1}$$

depends only on the adiabatic surface temperature. Despite the enhanced mixing away from the wall, in the unsteady simulation η remains near unity until near the trailing edge.

In these incompressible computations, temperature is a passive scalar. The contour levels in the figures could be regarded as ranging from 0 in the coolant stream to 1 in the gas stream. Dark regions show where the temperature is low.

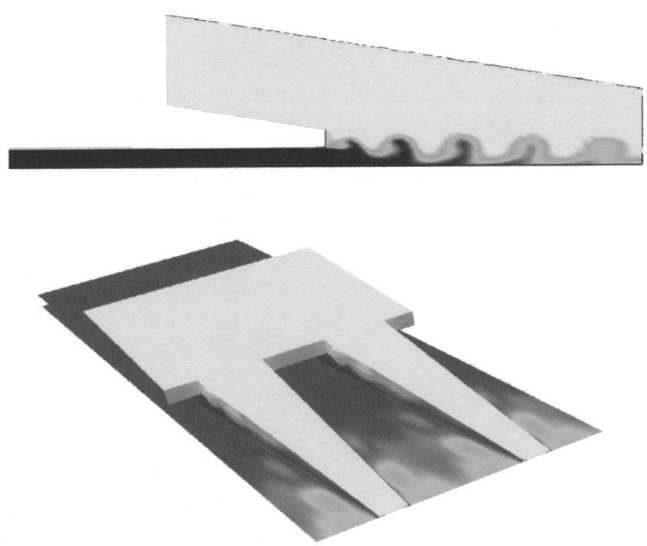

Fig. 4 Temperature contours illustrating natural unsteadiness. Side view and wall temperature under natural unsteadiness.

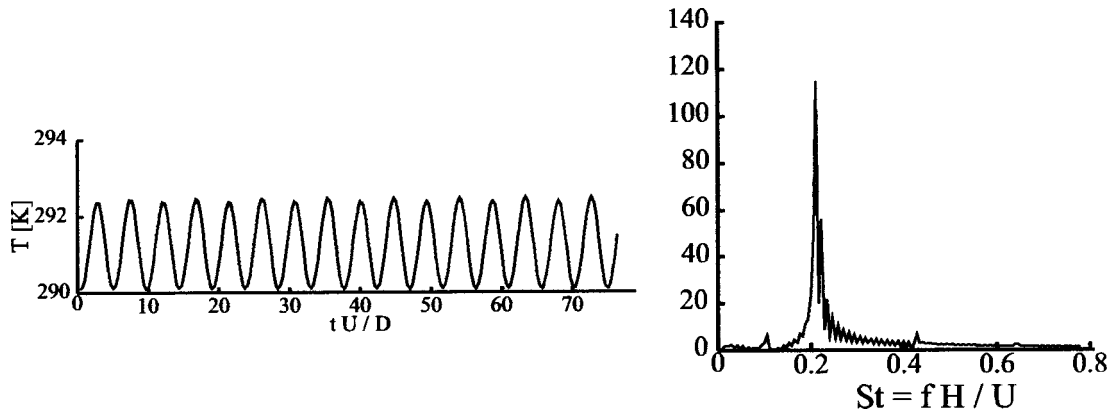

Fig. 5 A sample time history and spectrum

The plan form in Fig. 4 illustrates this more completely. Hot fluid is seen on top of the land. This is carried over the land, and is not cooled by mixing with the jet; but the lower surface, between the lands, remains near the jet temperature to the trailing edge. Hot fluid begins to impinge near the vertical walls of the land.

Time histories of temperature near the lower wall show the strict periodicity. This demonstrates that the computation has converged to a limit cycle. Spectra contain a sharp peak at a Strouhal number of 0.2 based on the nozzle lip thickness (Fig. 5). In reference to Fig. 1, the spike in Fig. 5 is the coherent unsteadiness; it is resolved as part of the mean flow. The broadband is not simulated; it is represented by the Reynolds-averaged turbulence model.

The extra mixing due to unsteadiness motivated a further study in which the velocity at the inlet to the plenum was pulsated:

$$U_{\text{in}} = U_0(1 + A \sin \omega_f t).$$

Although the forcing frequency, ω_f, was varied, the largest and most interesting response was for $\omega_f H/U = 0.2$; i.e., forcing with the natural shedding frequency. A was also varied. The value $A = 0.1$ is selected as representative of cases where forcing has a pronounced effect.

Figure 6 contains a time history and spectrum for the flow produced by inlet pulsations. Rather curiously, the response contains a strong subharmonic of the forcing frequency, and even a sub-subharmonic. The period is four times that of the forcing. On close inspection, a very weak subharmonic is seen, even in the natural case of Fig. 5; it becomes quite pronounced with forcing. The flow structure responsible for the appearance of subharmonics will be discussed below.

Again, the time history in Fig. 6 shows that we are simulating a periodic, ensemble-averaged flow. The chaotic, broadband component is represented by the closure model. There is no randomness in the time history; in particular, this is not a turbulent eddy simulation. That point should be emphasized: there is no connection between the present unsteady RANS computations and large eddy simulation (LES). The latter simulates random fields and would have to be phase averaged to extract coherent unsteadiness. That would require an extremely expensive computation, that included several hundred periods to obtain statistical convergence.

The influence of the plenum pulsations on mixing is protrayed in Fig. 7. Mixing now brings heated fluid to the wall a couple of nozzle diameters downstream. The pattern of wall temperature, in the lower part of Fig. 7, shows a distinct change in the distribution of mixing. The highest temperature now occurs on the midline, between the lands. The warmer fluid is swept down in the central region of the lower wall, leaving a small region next to the lands at the cold temperature.

The centerline effectivenesses for the three cases of steady, natural unsteadiness, and forced unsteadiness are plotted in Fig. 8 versus the distance between the slot breakout and trailing edge. The forced case shows a significant decline in effectiveness, beginning shortly after the nozzle exit. It was the intention of this simulation to produce mixing that resembled lab tests. The data in Fig. 8 are from Holloway et al. [1].

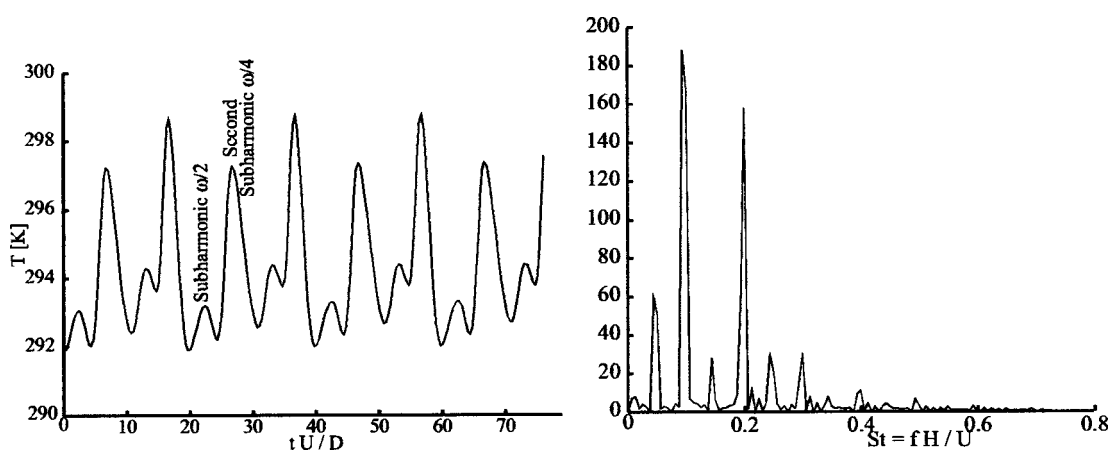

Fig. 6 A sample time history and spectrum, with forcing

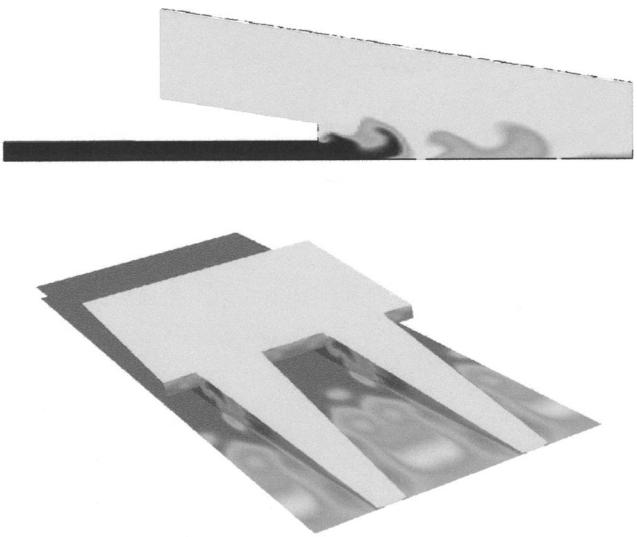

Fig. 7 Temperature contours with forced unsteadiness. Side view and wall temperature under forcing.

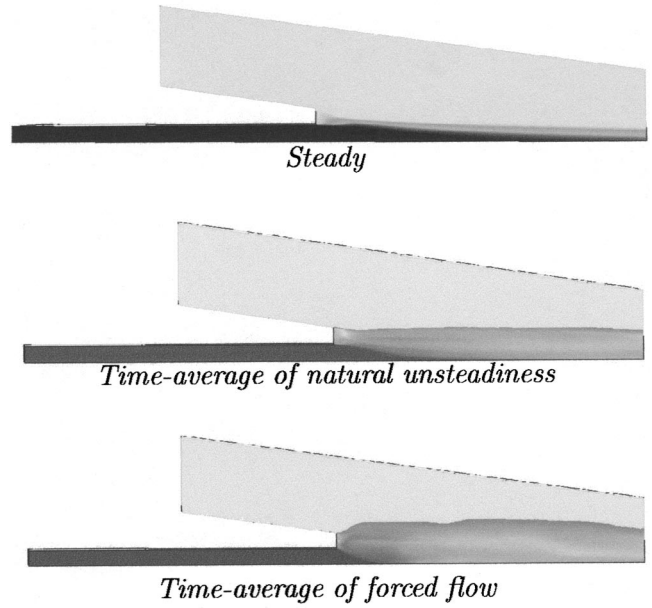

Fig. 9 Time-averaged temperature contours in a midspan plane

While it is unlikely that simple, plane wave forcing occurred in the lab, both η and the spatial pattern of heating in Fig. 7 very closely mirror those seen in experiments. To repeat a previous disclaimer, this simulation is not being presented as a prediction method. It illustrates the role that mean flow unsteadiness and three-dimensionality can play in trailing edge coolant flows.

The time-averaged, unsteady midspan temperature fields are compared to the steady computation in Fig. 9. The contribution of coherent unsteadiness is enhanced mixing. The steady computation represents mixing by broadband turbulence alone (via the turbulence model). The natural vortex street wafts the mixing layer, spreading the time-averaged temperature field. The evolution is similar to the steady case, but with faster spreading. Forcing produces stronger periodic, steamwise vortices. These change the nature of mixing. Heat disperses more quickly and the layer between free-stream and jet temperature is disrupted. A well-mixed region forms near the wall.

The drastic change in mixing that accompanies unsteadiness warrants explanation. Its origin is in the vortical features that occur in the jet. The following observations are presented for the purpose of uncovering some of the physical mechanisms that are at work.

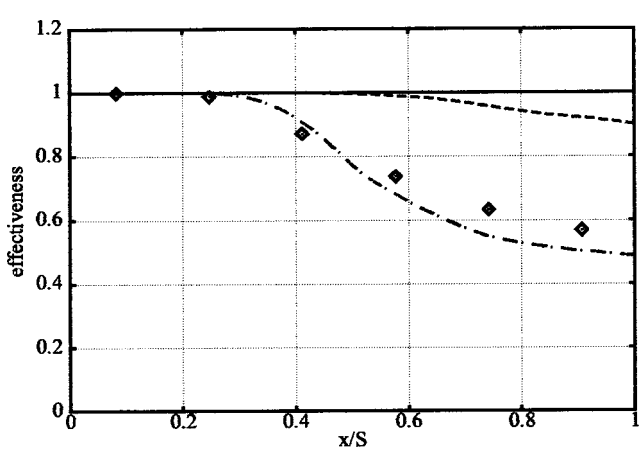

Fig. 8 Centerline adiabatic effectiveness. —, steady; ----, natural shedding; –––, forced. ♦, experiments from Holloway et al. [1].

The unsteadiness is associated with quite complex flow patterns. The midspan sections (Figs. 4, 7) are misleading in their simplicity: the flow is highly three-dimensional. The midspan sections have the appearance of shedding from a blunt trailing edge. While it is obvious that a two-dimensional geometry will produce a von Kàrmàn vortex street, it is far from obvious in three dimensions; indeed, three-dimensionality can suppress coherent shedding. In fact, a modification to the present geometry produced that effect.

The question arose as to whether the natural frequency is peculiar to the present geometry. To an extent it is. The present geometry was simplified to a series of rectangular wall jets in coflow by removing the protruding section of the lands. Simulations then converged to steady flow, even though they were computed with time accuracy. Grid- and time-step refinements on the truncated land geometry always converged to steady flow.

These results are consistent with the observation by Martini and Shultz [5] that coherent unsteadiness was not significant in their geometry—which did not have lands. This might not be surprising. The unsteadiness originates at the upper wall of the breakout. The jets are not the cause of unsteadiness; rather, they break up

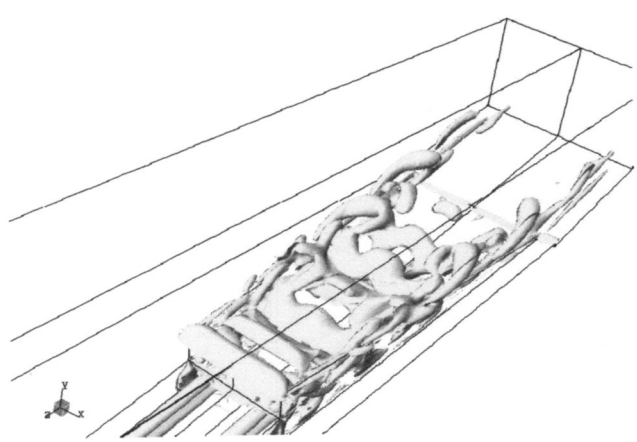

Fig. 10 Vortices with natural unsteadiness

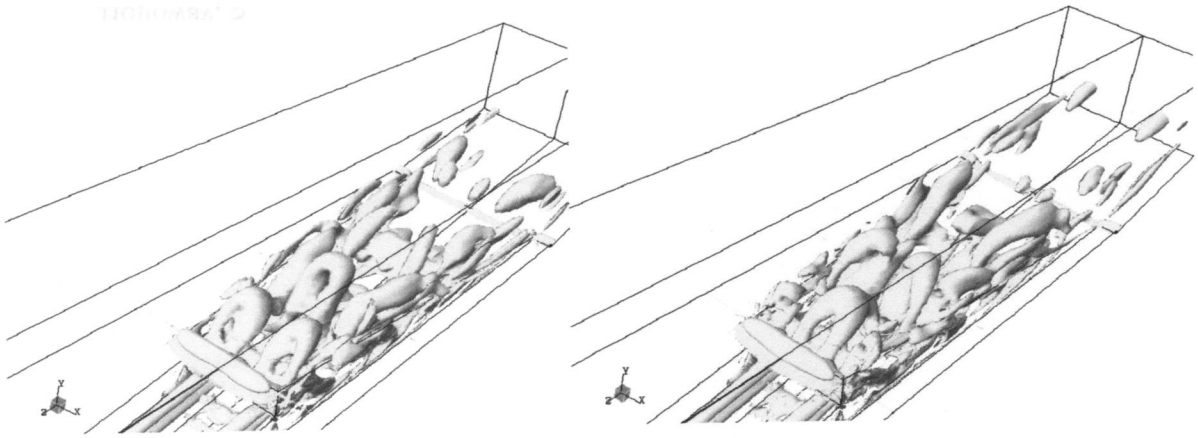

Fig. 11 Vortices with forced unsteadiness. Two instants, showing the origin of subharmonics.

the spanwise coherence of the flow leaving the upper surface, above the nozzles; i.e., three-dimensionality suppresses unsteadiness. The surprising observation is that the protruding lands restores coherent unsteadiness. The protruding section seems to impose a spanwise periodicity that resynchronizes the vortex shedding from the upper and lower surfaces of the nozzle lip.

A perspective on the flow complexity is provided by vortex visualization. Figures 10 and 11 show the three-dimensional vortex streets with natural and forced unsteadiness. A surface $Q>0$ is plotted, where $Q\equiv|\Omega|^2-|S|^2$, with S and Ω being the rate of strain and rate of rotation tensors. Inside these surfaces, the rate of rotation is larger than the rate of strain: that is the sense in which Q detects vortices. Note that a full jet nozzle was created in these figures by reflecting the computational domain across the symmetry plane—solely for the purpose of display. As complex as the vortical structure appears to be, this is not a turbulent eddy simulation: the vortex pattern repeats periodically and represents the ensemble-averaged flow.

The natural unsteadiness (Fig. 10) takes the form of vortex tubes, with strong three-dimensionality only occurring near the vertical walls of the lands. The connection to a two-dimensional, von Kàrmàn street is apparent. The three-dimensionality due to the wall jets is not disruptive of shedding.

A horseshoe vortex wraps around the junctions between the upstream edge of the land and the upper and lower walls in the plenum portion of Fig. 2. This vortex can be seen exiting the jet at the bottom of Fig. 10. These horseshoe vortices may contribute to the distortion of the shed vortices near the end walls in the case of natural unsteadiness. However, they do not seem to make a major contribution to mixing beyond the nozzle exit.

The forced case, in Fig. 11, is more intriguing. The shedding now breaks into vortex loops. The subharmonic component in the spectrum seems to be due to the loops appearing alternatively at the sides and in the middle of the slot. This can be seen by comparing the figures at the left and the right; they are one natural period apart in time. Again, it must be emphasized that, as complex as the flow may seem to be, it repeats periodically; this is not a LES.

The mean flow vortices now have a stronger streamwise component than in the unforced case. Streamwise vorticity is known to greatly enhance mixing in shear layers [6]. The surface temperature patterns in Figs. 4 and 7 reflect the role of streamwise vortices. In Fig. 4, higher wall temperatures occur near the lands because that is where the streamwise vortices occur. In the forced case, Fig. 7, vortex loops in the middle of the flow result in the higher wall temperatures.

These simulations raise the intriguing possibility of reducing mixing and improving cooling via control of the unsteadiness. Because the mean flow unsteadiness is at issue, this does not require suppression of turbulence; the broadband, turbulent component does not mix the hot stream to the wall. Passive devices might be able to break the coherence and suppress mixing. We have seen that modifications to the land geometry downstream of the nozzle breakout can have this effect.

Acknowledgment

This work was sponsored by General Electric aircraft engines through their Universities Strategic Alliance. We are especially grateful to Scott Hunter, Fred Buck, and Ganesh Kumar for their advice.

References

[1] Holloway, S. D., Leylek, J. H., and Buck, F. A., 2002, "Pressure-Side Bleed Film Cooling: Part I, Steady Framework for Experimental and Computational Results," ASME Turbo Expo 2002; papers GT-2002-30471.
[2] Iaccarino, G., Ooi, A., Durbin, P. A., and Behnia, M., 2003, "Reynolds Averaged Simulation of Unsteady Separated Flow," Int. J. Heat Mass Transfer, **24**, pp. 147–156.
[3] Holloway, S. D., Leylek, J. H., and Buck, F. A., 2002, "Pressure-Side Bleed Film Cooling: Part 2, Unsteady Framework for Experimental and Computational Results," ASME Turbo Expo 2002, papers GT-2002-30472.
[4] Rigby, D. L., and Bunker, R. S., 2002, "Heat Transfer in a Complex Trailing Edge Passage for a High Pressure Turbine Blade," NASA/CR 2002-211701.
[5] Martini, P., and Shultz, A., 2004, "Experimental and Numerical Investigation of Trailing Edge Film Cooling by Circular Coolant Wall Jets Ejected From a Slot With Internal Rib Arrays," ASME J. Turbomach., **126**, pp. 229–236.
[6] Moser, M. M., and Rogers, R. D., 1991, "Mixing Transition in the Cascade to Small Scales in a Plane Mixing Layer," Phys. Fluids A, **3**, pp. 1128–1134.